3D-QSAR and molecular modeling studies on 2,3-dideoxy hexenopyranosid-4-uloses as anti-tubercular agents targeting alpha-mannosidase

ARTICLE *in* BIOORGANIC CHEMISTRY · FEBRUARY 2015

Impact Factor: 2.15 · DOI: 10.1016/j.bioorg.2015.02.001

9 AUTHORS, INCLUDING:

Priyanka Shah

Banasthali University

24 PUBLICATIONS **160** CITATIONS

SEE PROFILE

Mohammad Saquib

University of Allahabad

20 PUBLICATIONS **125** CITATIONS

SEE PROFILE

Vinayak Singh

University of Cape Town

8 PUBLICATIONS **28** CITATIONS

SEE PROFILE

Arun K Shaw

Council of Scientific and Industrial Researc…

66 PUBLICATIONS **735** CITATIONS

SEE PROFILE

Bioorganic Chemistry 59 (2015) 91–96

Contents lists available at ScienceDirect

Bioorganic Chemistry

journal homepage: www.elsevier.com/locate/bioorg

3D-QSAR and molecular modeling studies on 2,3-dideoxy hexenopyranosid-4-uloses as anti-tubercular agents targeting alpha-mannosidase

Priyanka Shah [a,1], Mohammad Saquib [b,1,2], Smriti Sharma [b], Irfan Husain [b], Sandeep K. Sharma [c], Vinayak Singh [c], Ranjana Srivastava [c], Arun K. Shaw [b,*], Mohammad Imran Siddiqi [a,*]

[a] Molecular and Structural Biology Division, CSIR-Central Drug Research Institute (CDRI), Lucknow 226031, India
[b] Medicinal and Process Chemistry Division, CSIR-Central Drug Research Institute (CDRI), Lucknow 226031, India
[c] Microbiology Division, CSIR-Central Drug Research Institute (CDRI), Lucknow 226031, India

ARTICLE INFO

Article history:
Received 1 October 2014
Available online 11 February 2015

Keywords:
Homology modeling
Docking
Molecular dynamics
CoMFA
CoMSIA
Hierarchical clustering

ABSTRACT

Ligand-based and structure-based methods were applied in combination to exploit the physicochemical properties of 2,3-dideoxy hex-2-enopyranosid-4-uloses against *Mycobacterium tuberculosis* H37Rv. Statistically valid 3D-QSAR models with good correlation and predictive power were obtained with CoMFA steric and electrostatic fields ($r^2 = 0.797$, $q^2 = 0.589$) and CoMSIA with combined steric, electrostatic, hydrophobic and hydrogen bond acceptor fields ($r^2 = 0.867$, $q^2 = 0.570$) based on training set of 33 molecules with predictive r^2 of 0.808 and 0.890 for CoMFA and CoMSIA respectively. The results illustrate the requirement of optimal alkyl chain length at C-1 position and acceptor groups along hydroxy methyl substituent of C-6 to enhance the anti-tubercular activity of the 2,3-dideoxy hex-2-enopyranosid-4-uloses while any substitution at C-3 position exert diminishing effect on anti-tubercular activity of these enulosides. Further, homology modeling of *M. tuberculosis* alpha-mannosidase followed by molecular docking and molecular dynamics simulations on co-complexed models were performed to gain insight into the rationale for binding affinity of selected inhibitors with the target of interest. The comprehensive information obtained from this study will help to better understand the structural basis of biological activity of this class of molecules and guide further design of more potent analogues as anti-tubercular agents.

1. Introduction

Today tuberculosis (TB) continues to be one of the leading causes of death globally, from a single infectious agent [1–3]. The recent emergence of multi-drug resistant TB (MDR-TB), extensively drug resistant TB (XDR-TB) and co-infection with HIV have rendered the existing chemotherapeutic approaches progressively ineffective [4] raising fears that TB may become uncontrollable [5]. This has prompted a new sense of urgency toward the search of novel chemical entities as anti-TB molecules having potent activity, reduced toxicity, rapid mycobactericidal action, shortened duration of therapy and new site of action to minimize the chances of drug resistance [6,7]. In recent decades there has been a renewed interest in the use of carbohydrates scaffolds in drug discovery due to their unique properties [8]. However, a major impediment in the development of carbohydrate molecules as therapeutics has been their rapid degradation in the body by glycosidases. One way to overcome this pharmacokinetic difficulty is to use modified sugars which may not be recognized by the regular complement of glycosidases present in the body [9,10]. In this milieu, we recently reported the design and synthesis of 2,3-dideoxy hex-2-enopyranosid-4-uloses which are small, modified sugar molecules as promising anti-tubercular agents [11].

1.1. Ligand-based molecular modeling

Quantitative structure activity relationship (QSAR) can offer some valuable suggestions to improve the drug activity on the basis of QSAR analyses fitted to the activity data of training set of molecules aligned in three dimensional spaces [12–15]. Therefore, ligand based 3D-QSAR models were built using Comparative Molecular Field Analysis (CoMFA) [16] and Comparative Molecular Similarity Indices Analysis (CoMSIA) [17] to understand the key

* Corresponding authors.
E-mail address: mi_siddiqi@cdri.res.in (M.I. Siddiqi).
[1] Joint first authors.
[2] Present affiliation: Department of Chemistry, University of Allahabad, Allahabad - 211002, U.P., India.

http://dx.doi.org/10.1016/j.bioorg.2015.02.001
0045-2068/

structural elements capable to produce more effective inhibitors. Moreover, training set used to develop the predictive QSAR model is supposed to encompass diverse chemical entities as much as possible to train highly predictive models [18]. According to Maggiora and Johnson similarity–property principle [19], chemical similarity among molecules can be related to the biological activity. This correlation is mostly dependent on the method of similarity measures used in the study and varies between different methods which are classified according to the information used to calculate the similarity between two structures [20,21]. Structural or topological fingerprints, like [22] are simple and rapid methods to encode the information in the form of fingerprints based on features that are included in the structures. These fingerprints can be used to measure the degree of dissimilarity between all pairs of molecules to build a diversified training set. Therefore, to rationalize the selection method in the current study, training set of 33 molecules and test set of 5 molecules were selected from clusters built from hierarchical clustering using pvclust [23] R package to ensure the molecular diversity in both the training and test sets. 2D descriptors [22] were utilized in calculating dissimilarity matrix to cluster the whole dataset.

1.2. Structure-based molecular modeling

On the other hand, structure-based drug design depends entirely on information obtained from three dimensional structures of the biological targets of interest. The proper analyses of spatial arrangements of ligands present in the protein's active site can offer valuable rationale for activity profile of structural analogs in terms of favorable and unfavorable intermolecular interactions. We obtained the inhibition activity of three inhibitors from the present dataset against the alpha-mannosidase enzyme where one of the compounds corresponds to the most active anti-tubercular among other compounds in this dataset.[24] In the absence of X-ray crystallographic structure of the protein, homology modeling was attempted to generate three-dimensional coordinates of the target protein *Mycobacterium tuberculosis* alpha-mannosidase. Cloning and expression studies of Rv0648 gene have demonstrated in previous studies that activity of alpha-mannosidase is important for biosynthesis of mannosylated glycoconjugates in *M. tuberculosis* [25]. Sequence annotation shows that alpha mannosidase enzymes belong to the family of 38 glycosyl hydrolase and catalyze the cleavage of alpha-mannose. Due to the limited sequence similarity with full protein, homology model has been generated only for alpha-mannosidase domain. This model is further used for docking of selected inhibitors followed by nanosecond duration molecular dynamics simulations. Biological activities of three selected inhibitors against *M. tuberculosis* alpha mannosidase were considered in the present study to understand the molecular basis of rationalization behind binding affinity.[24] On the basis of ligand based QSAR analyses in conjunction with molecular docking and molecular dynamics (MD) simulations on homology model of alpha mannosidase co-complexed with inhibitors, key points were highlighted which can act as guidelines for design of new inhibitors against *M. tuberculosis* alpha-mannosidase.

2. Materials and methods

2.1. Ligand-based studies

Thirty-eight molecules from our previously reported work [11] (Table S1) with MIC values <25 μg/mL were converted to the corresponding pMIC (-log MIC) to be used as dependent variable for developing the 3D-QSAR model. Correct alignment of selected conformations of molecules is the most crucial step of development of reliable 3D-QSAR models. Therefore, global energy minimum conformation of most active compound **38** was obtained through the simulated annealing where molecule was heated up to 700 K for 1000 fs followed by annealing the molecule to 200 K for 1000 fs and, further followed by BFGS energy minimization. This energy minimized molecule was used as the alignment template, and the rest of the molecules were built and aligned on it subsequently by using the database alignment module (Fig. 1) using Tripos force field [26] and Huckel partial atomic charges implemented in [27]. Further, the dissimilarity matrix was built between all pairs of compounds measured by tanimoto similarity coefficient between the MACCS fingerprints calculated from rcdk package [28]. Hierarchical clustering was done using ward's linkage method [29] for all the thirty-eight molecules using R 2.12.2 package available at [30] to remove subjective bias in the variable selection procedure. Approximately unbiased (AU) *p*-values were obtained via multiscale bootstrap resampling for clusters using pvclust package in R 2.12.2 for assessing the uncertainty in hierarchical cluster analysis. Three-dimensional quantitative structure–activity relationships (3D-QSAR) methodologies: comparative molecular field analysis (CoMFA) [31] and comparative molecular similarity indices analysis (CoMSIA) [31,32] were applied with default values of different parameters on the training set molecules divided on the basis of clustering. Further, the predictive correlation coefficient (r^2_{pred}) based on the test molecules, is computed by using formula

$$r^2_{\text{pred}} = (\text{SD} - \text{PRESS})/\text{SD}$$

where SD is the sum of the squared deviations between the biological activities of the test set and mean activities of training set molecules and PRESS is the sum of squared deviation between predicted and actual activity for every molecule in test set.

2.2. Receptor-based studies

Amino acid sequence for *M. tuberculosis* alpha mannosidase (Uniprot id: P96937) was evaluated further to determine the presence of conserved domains or signature sequences using Interpro (http://www.ebi.ac.uk/interpro/) and pfam (http://pfam.sanger.ac.uk/) databases. The server for homology detection, HHpred [33] which utilizes hidden markov model to search for suitable templates by profile–profile alignment methods together with predicted secondary structure to produce a high quality alignment even for distant homologs, was used for template searching. Next, a multi-template alignment with selected templates (PDB id: 3BVX and 3LVT) together with zinc and swainsonine co-complexed PDB 2WYI was used by modeler 9.10 [34] to generate ten 3D coordinates of the *M. tuberculosis* alpha-mannosidase. Top model was selected on the basis of Dope score and checked by procheck for presence of structural discrepancies. Low complexity regions with no similarity with templates were deleted and rest of the portion was considered for further studies. Zinc binding site was confirmed

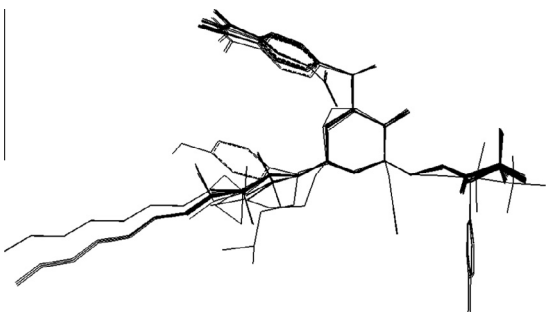

Fig. 1. Database alignment of 38 molecules used in QSAR studies.

on the basis of alignment with template molecules, sequence conservation and metal binding site prediction server CHED (http://ligin.weizmann.ac.il/~lpgerzon/mbs4/mbs.cgi).

Further, docking of compounds **1**, **4**, **38** with known activity against alpha-mannosidase (Table S1) was performed by Autodock 4.2 on homology model of alpha-mannosidase. Kollman charges were assigned to all protein atoms. Grid was centered at zinc binding site and prepared with $40 \times 40 \times 40$ grid points of 0.375 Å spacing and 100 runs were performed for each docking. Rest of the settings were standard in Autodock 4. To validate the sensitivity of docking parameters toward zinc-binding protein, swainsonine was redocked into template PDB 2WYI complexed with zinc and swainsonine in X-ray crystallographic structure.

Further, molecular dynamics simulations were performed on homology model of alpha mannosidase complexed with docked conformations of inhibitors **1**, **4** and **38** (Table S1) to check the stability of complexes over time using GROMACS 4.5 with GROMOS 96 53a1 forcefield. During simulations, protein–inhibitor complexes including divalent zinc metal ion were surrounded by cubic box extended 10 Å with periodic boundary conditions in all the direction from the protein and filled with SPC water molecules. The zinc coordinated histidine was treated as neutral with hydrogen on ND1. The systems were neutralized by adding Na+ and Cl− counter ions replacing the water molecules followed by energy minimization of the systems by steepest descendent followed by conjugant gradient method. Then equilibrium MD simulations at constant temperature (NVT) for 50 picosecond followed by 50 picoseconds of equilibrium MD simulations at constant pressure (NPT) were performed. After sufficient equilibration, full MD run was performed. Classical mechanics are not very accurate when it comes to dealing with the problem of calculating polarization and charge transfer effect of ions in protein. Therefore, distance restraints were imposed on zinc and its coordinating atoms to maintain the correct ligation state of zinc ion present in the active site of homology model [35]. The distance constraints were set such that whenever the distance between zinc ion and its coordinating atoms increased by more than 0.1 nm beyond the starting model, a force started acting on the system with force constant of 1000 kJ/mol nm^2. Therefore, restraining forces are zero in the starting conformation and forces started acting as the metal coordinating atoms displace from their original place. Although, some other methods were also found in literature to deal with ion ligation using stronger forces or covalent bonds but such models may reduce the desired flexibility of the systems. During the full MD run, energies and coordinates were saved once every two picoseconds. V-rescale temperature coupling and Parrinello Rahman pressure coupling were used. Long range electrostatics was simulated using the particle-mesh Ewald method, whereas Van der Waals cut-off of 1.4 nm was used. Neighbor list was updated every 5 fs.

Table 1
Distribution of molecules into different clusters.

Cluster name	Compound number
Cluster 1	1, 2, 3, 4, 7, 8, 9, 10, 14, 15, 16, 18, 23, 27, 32, 33, 34, 35, 37
Cluster 2	5, 6, 11, 12, 24, 25, 26, 28, 29, 30, 31, 36, 38
Cluster 3	13, 17, 19, 20, 21, 22

3. Results and discussion

3.1. Ligand-based studies

To better understand the relationship between structure and activity of the molecules, a dataset of our recently synthesized thirty-eight 2,3-dideoxy hex-2-enopyranosid-4-uloses with anti-tubercular MIC activity values was used for 3D QSAR studies [11]. Homogeneous distribution of all chemical classes of compounds in training set and test set for internal and external validation was ensured by hierarchical clustering using the ward method into three clusters of significant sizes on the basis of tanimoto similarity between all pairs of molecules using MACCS molecular fingerprints. Degree of uncertainty of different parameters of hierarchical clustering method was assessed by an R package, pvclust with number of bootstrapping [36,37] 1000. Pvclust provides two types of *p*-value to assess the resultant clusters: AU [38,39] (approximately unbiased) *p*-value which is computed by multi-scale bootstrap resampling and BP (Bootstrap Probability) value computed by normal bootstrap resampling. The AU value calculated using the multi-scale bootstrap techniques have been found to be less biased than conventional BP (bootstrap probability) [40]. Therefore, AU values were used to prioritize molecular fingerprinting method among available choices (standard, extended, estate and maccs) in rcdk. Clusters highlighted by red rectangles in Supplementary Fig. S1 denoting AU larger than 95% (colored in red) values written on the edges. Clustering of MACCS method of molecular fingerprint was selected as preferred method as it was showing even distribution of molecules among clusters with lower standard error value and higher AU *p*-values for all the molecules (Supplementary Figs. S1 and S2). We obtained 3 clusters listed in Table 1 containing 19, 13 and 6 molecules respectively. Test set was built by randomly choosing 2 molecules from each of the 2 bigger clusters containing 13 and 19 molecules respectively and 1 molecule from smaller cluster of total 6 molecules and rest of the 33 molecules were included in the training set for PLS analysis.

3.2. QSAR analysis

Satisfactory 3D-QSAR models were obtained with the selected training set of molecules. The predicted activities for the inhibitors versus their experimental activities listed in Table S1 demonstrate that the predicted activities are in good agreement with the experimental data for all the generated models (Fig. 2). The statistical parameters obtained from CoMFA and CoMSIA models are summarized the Table 2. For PLS analysis, optimum numbers of components were obtained from cross-validation calculation with

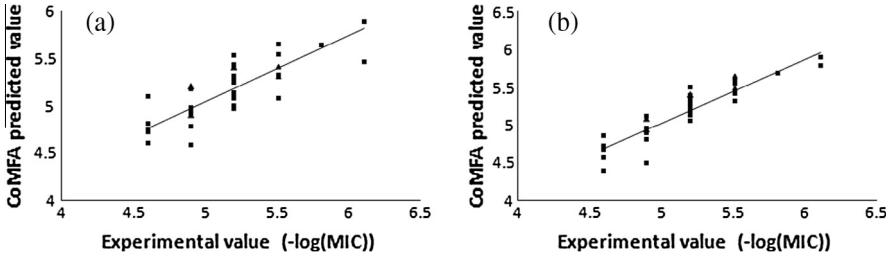

Fig. 2. Correlation between the predicted values vs experimental value for training (♦) and test set (▲) compounds by CoMFA (a), and CoMSIA (b).

Table 2
Summary of the CoMFA and CoMSIA statistical results for the training set molecules.

	CoMFA	CoMSIA
q^2 (leave-one-out)	0.637	0.551
q^2 (cross-validated)	0.867	0.570
r^2	0.797	0.867
SEE[a]	0.207	0.172
N_c[b]	6	7
Field contribution (%)		
Steric	0.665	0.285
Electrostatic	0.335	0.267
Hydrophobic		0.326
HB donor		
HB acceptor		0.121

[a] Standard error of estimate.
[b] Optimum number of components.

lower standard error of estimate (SEE) while considering predictability of test set molecules of models also.

For CoMFA, optimum number of components was 6 with $q^2_{\text{leave-one-out}}$ value 0.637 while the non-cross-validated PLS analysis with the optimum principle component (PC) revealed a conventional r^2 value of 0.797, $F = 17.055$, and a standard error of estimate (SEE) of 0.207. In case of CoMSIA analysis, it was found that the presence of hydrogen bond donor field does not help in improving the performance of QSAR model. Therefore CoMSIA model was constructed using four fields (steric, electrostatic, hydrophobic and hydrogen bond acceptor). An excellent value of 0.867 for r^2_{nv}, an *F*-value of 23.223, 0.570 for r^2 cross-validation with 7 optimum numbers of components and r^2_{pred} of 0.890 were obtained for CoMSIA model. The contribution of steric, electrostatic, hydrophobic, and hydrogen bond acceptor fields of this model were 29.1%, 21.6%, 35.0% and 14.3% respectively. Moreover, high value of bootstrapped r^2 of 0.887 ± 0.022 and 0.891 ± 0.040 with SEE_{boot} of 0.156 ± 0.084 and 0.134 ± 0.078 shows good internal consistency in the CoMFA and CoMSIA QSAR models respectively. The percent contribution of field descriptors of CoMFA and CoMSIA models obtained from non-cross validation show that steric and hydrophobic field contributions are quite important factor for potency of these molecules as compared to other descriptors.

3.3. Contour analysis

The results obtained from CoMFA and CoMSIA PLS models were graphically interpreted through the color coded contour maps obtained after contour analysis for deriving relationship between molecular field differences of a set of urolase derivative molecules and differences in their biological activities. Highly active compound was embedded in the CoMFA and CoMSIA contour maps to demonstrate its affinity for the steric, electrostatic, hydrophobic and hydrogen bond donor regions of inhibitors (Figs. 3 and 4).

From steric and electrostatic contours analysis of CoMFA and CoMSIA, it is clearly visible that the presence of optimal size and length of steric groups around C-1 play very significant role while substitution with electron acceptor group at C-6 position of enones would help in enhancing activity. One big green contour trailed by yellow contour in Fig. 3b highlights the requirement of the optimal chain length of -Oalkyl substituents attached to the C-1 of the enones. Compounds **14**, **23**, **27**, **32**, **33** and **34** with short chain length and compounds **5**, **18**, **21** and **36** with long -Oalkyl chains at C-1 position exhibited decreased activities compared to those of compounds **3**, **11**, **19**, **29**, **30**, **31**, and **38**. It is noteworthy here that any substitutions are not supported at C-3 position. Two yellow contours nearby C-3 position indicates unfavorability for steric bulks as shown in Fig. 3a as well as a big yellow hydrophobic unfavorable contour demonstrated in Fig. 4a indicates less favorability for bulky hydrophobic substituents. On the other hand presence of hydrogen bond acceptor groups are also not suitable in the vicinity of the C-3 substituents in the enones as shown by red colored contours of hydrogen bond acceptor unfavored region in Fig. 4b as obvious from the activity data of compounds **14**–**16**, **23** and **24**.

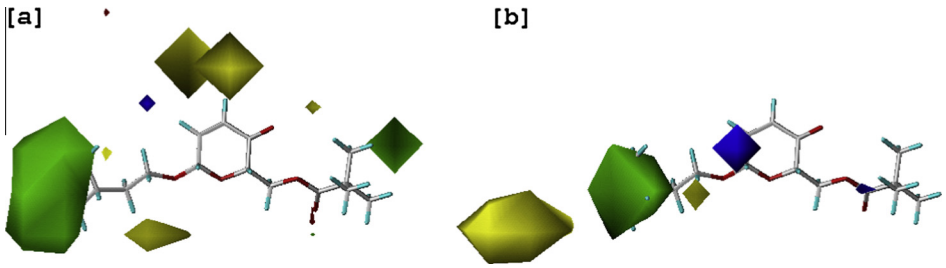

Fig. 3. (a) CoMFA and (b) CoMSIA steric (green favorable, yellow unfavorable) and electrostatic (blue electropositive, red electronegative) contour maps put onto most active molecule compound **38**.

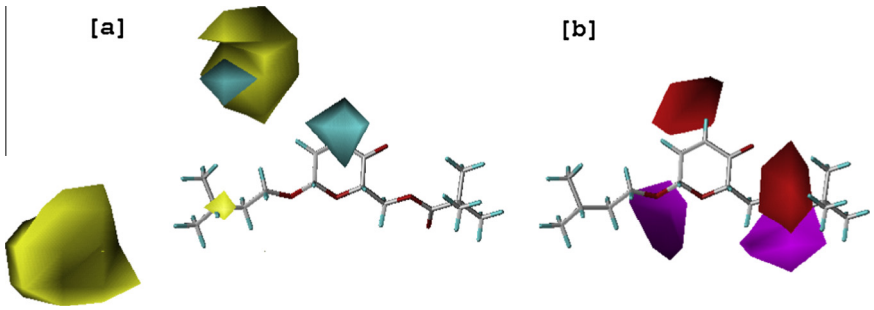

Fig. 4. CoMSIA (a) hydrophobic (cyan favorable, yellow unfavorable) and (b) hydrogen bond acceptor (magenta favorable, red unfavorable) contour maps onto compound **38**.

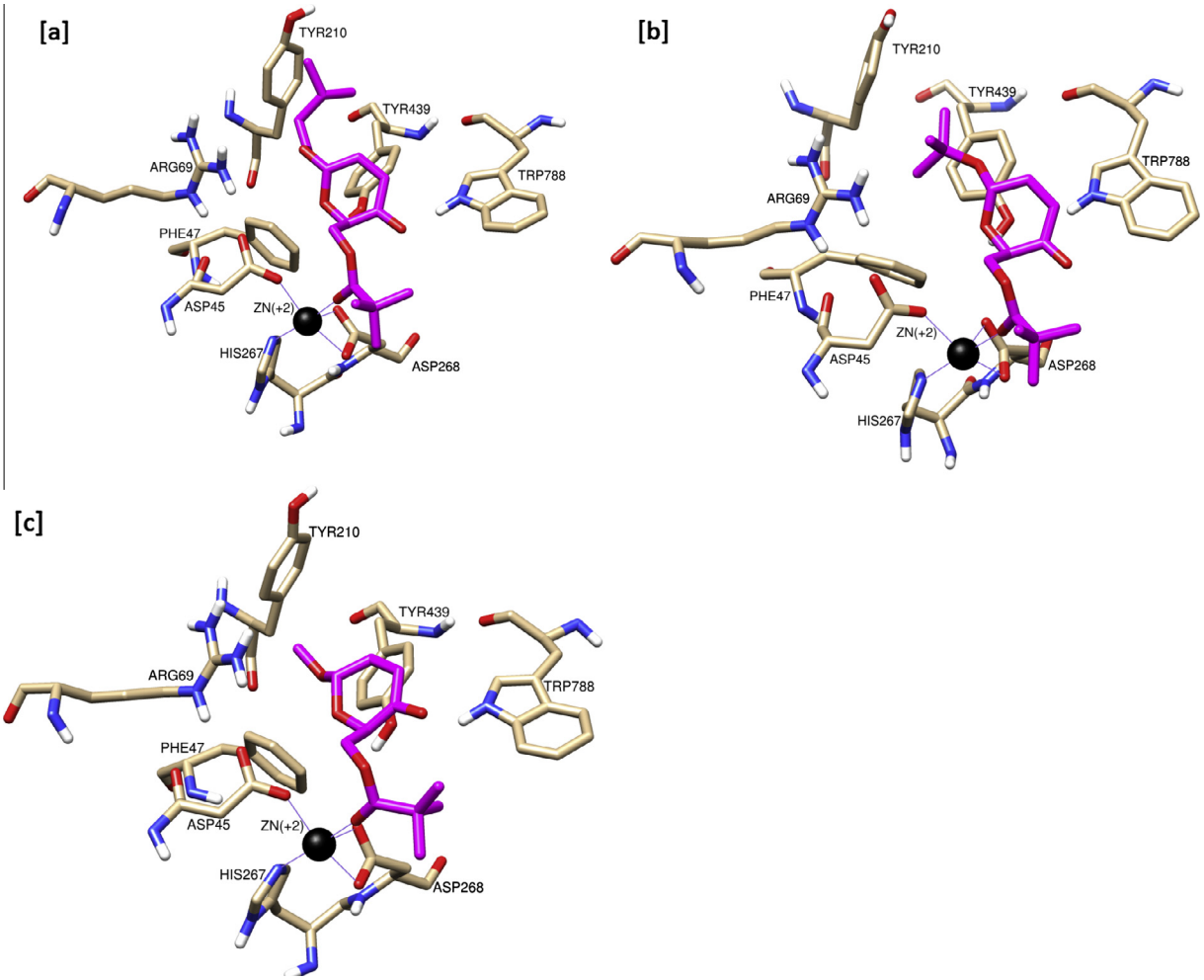

Fig. 5. The active site of *M. tuberculosis* alpha-mannosidase with (a) compound **38** (b) compound **4** and (c) compound **1**.

Two large size magenta color contours show favorability for hydrogen bond acceptor groups around the ether and ester containing side chains at positions C-1 and C-6 respectively.

3.4. Receptor-based studies

Sequence annotation from Interpro shows that modeled enzyme contains zinc dependent Glycoside hydrolase, family 38 comprises of three domains: N-terminal domain (residues 2–210), central domain (residues 212–283) and C-terminal domain (residues 314–525 and residues 751–946). Interproscan revealed that central domain and C-terminal domain of this protein sequence are interrupted by two insertions with no known similarity to any domain families in Interpro or pfam database. In this work, only catalytic domain belonging to glycoside hydrolase family was modeled by MODELLER with lowest global DOPE score found to be −103291.859375. Subsequently, model was docked with the compounds **1**, **4** and **38** that were found to be a competitive inhibitor of alpha-mannosidase (Jack bean), with Ki values of 68 μM, 275 μM and 353.9 μM respectively, [24] using Autodock4 with top cluster representatives in all docking runs selected as final docked conformations for each inhibitor. Visual inspection of ligands bound pocket revealed that the active site is primarily formed by hydrophobic residues. In this case, all the inhibitors have shown similar binding mode in the active site including coordination with the zinc ion (Fig. 5). Docking of metalloprotease is a challenging task because of lack of appropriate force field parameters in docking tools. Therefore, stability of initial geometries obtained from dockings were subjected to further validation by MD protocols to explore the conformation sampling of the inhibitors in the active site in addition to analyzing dynamics of ligand interacting residues over

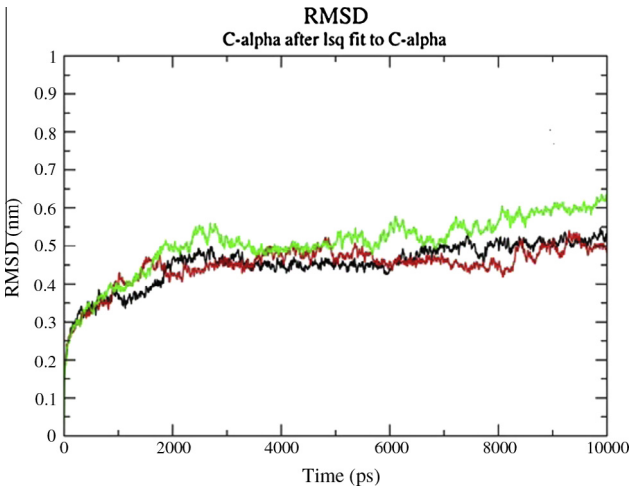

Fig. 6. C-α root mean square deviation (RMSD) of the three complexes: with compound **38**(black), compound **4** (red) and compound **1** (green).

time. MD simulation of 10 ns was performed to analyze the molecular basis of interaction between ligands and receptor over time. Zinc (+2) was found to be bonded in the active site in octahedral geometry during the full MD with RMSD in backbones was calculated to check the stability and consistency over time (Fig. 6). Although modeling only alpha-mannosidase domain would probably affect the overall stability of protein due to the absence of some important neighboring interactions. However, low RMSD values over time for the c-alpha atoms of protein docked with inhibitors as shown in Fig. 6, infer the stability of structure over time and thus overall accuracy of topology. Moreover, docked complex of most active compound **38** shows more consistency in conformation as deduced from low deviation in RMSD after a certain time during MD simulation study. Zinc bonding was assessed by measuring the distance between zinc and ligating atoms as a measure of coordinate bonding where distance between zinc and ligating atom is considered as bonded if distance between them is less than 3.2 Å. Then RMSD of angles between ideal and modeled geometries were used as assessment criteria for geometry of zinc in complexes. The zinc ion is found to be coordinated by OD2 of Asp45, NE2 of His267, OD1 and OD2 of Asp268, O of inhibitors and one of solvent molecule.

Ligand-based QSAR analysis has pointed to the significance of the acceptor and hydrophobic groups whereas MD simulations on homology model docked with selected inhibitors beautifully illustrate how these groups interact with active site residues and zinc. Similar modes of interactions with almost identical distances were observed over the time during simulations. Active site includes Asp45, Phe47, Arg69, His109, Tyr110, His267, Asp268, Gly272, Ser273, Glu274, Trp788, Asp790, Gln791, Pro792 and Arg794. We propose that pivaloyl group is involved in interactions important for protein–ligand complexation through metal–ligand chelation. While hydrophobic interaction is proposed to be favorable because of observed proximity of the alkoxy group to the aromatic chain of Trp788 and Phe47 protein residue.

Thus, intermolecular interaction analyses from MD simulations confirm the validity of contours obtained from ligand-based QSAR analysis. Green contours show the requirement of hydrophobic groups, necessary to interact with Gly272, Ser273 and Trp788 containing loop region while two hydrogen bond acceptor favoring contours represent the zinc coordinating groups. The current study thus attempted to characterize the 2,3-dideoxy hexenopyranosid-4-uloses as potent inhibitor of *M. tuberculosis* alpha mannosidase with proposal of statistically validated guidelines for designing of new inhibitors obtained from QSAR results rationalized on molecular basis of stability and interaction from molecular modeling studies.

4. Conclusion

Together with the statistical significance, good predictability and interpretability were achieved from the 3D-QSAR studies on a series of 2,3-dideoxy hex-2-enopyranosid-4-uloses used in this study. The constructed models provide valuable guidance for identification of steric and electrostatic properties as well as hydrophobic and acceptor hydrogen-bonding attributes that could play important role for the future development of even more potent 2,3-dideoxy hex-2-enopyranosid-4-uloses based anti-tubercular agents. Moreover, molecular modeling methods were utilized to enhance the understanding of substrate binding and catalytic mechanism. Both, ligand-based and structure-based results are in coordination with each other and validate the study for designing of more potent inhibitors of this class of compounds as anti-tubercular agents.

Acknowledgments

Works reported in this manuscript is supported by grants from CSIR network projects: SPLENDID (BSC0104) and GENESIS (BSC0121). PS thanks CSIR for SRF. This manuscript is CDRI communication number 8916.

Appendix A. Supplementary material

Supplementary data associated with this article can be found, in the online version, at http://dx.doi.org/10.1016/j.bioorg.2015.02.001.

References

[1] S.T. Cole, Microbiology 148 (2002) 2919–2928.
[2] H. Tomioka, K. Namba, Kekkaku 81 (2006) 753–774.
[3] Global tuberculosis control: epidemiology, strategy, financing: WHO report 2009 <http://www.who.int/tb/publications/global_report/2009/en/index.html>.
[4] A. Somoskovi, L.M. Parsons, M. Salfinger, Respir. Res. 2 (2001) 164–168.
[5] E. Vicente, R. Villar, A. Burguete, B. Solano, S. Perez-Silanes, I. Aldana, J.A. Maddry, A.J. Lenaerts, S.G. Franzblau, S.H. Cho, A. Monge, R.C. Goldman, Antimicrob. Agents Chemother. 52 (2008) 3321–3326.
[6] A. Koul, E. Arnoult, N. Lounis, J. Guillemont, K. Andries, Nature 469 (2011) 483–490.
[7] Y. Zhang, K. Post-Martens, S. Denkin, Drug Discov. Today 11 (2006) 21–27.
[8] W. Meutermans, G.T. Le, B. Becker, ChemMedChem 1 (2006) 1164–1194.
[9] A. Dove, Nat. Biotechnol. 19 (2001) 913–917.
[10] T.K. Ritter, C.H. Wong, Angew. Chem. Int. Ed. Engl. 40 (2001) 3508–3533.
[11] M. Saquib, I. Husain, S. Sharma, G. Yadav, V.K. Singh, S.K. Sharma, P. Shah, M.I. Siddiqi, B. Kumar, J. Lal, G.K. Jain, B.S. Srivastava, R. Srivastava, A.K. Shaw, Eur. J. Med. Chem. 46 (2011) 2217–2223.
[12] V. Virsdoia, M.S. Shaikh, A. Manvar, B. Desai, A. Parecha, R. Loriya, K. Dholariya, G. Patel, V. Vora, K. Upadhyay, K. Denish, A. Shah, E.C. Coutinho, Chem. Biol. Drug Des. 76 (2010) 412–424.
[13] A. Manvar, R. Pissurlenkar, V. Virsodia, K. Upadhyay, D. Manvar, A. Mishra, H. Acharya, A. Parecha, C. Dholakia, A. Shah, E. Coutinho, Mol. Divers. 14 (2010) 285–305.
[14] Shagufta, A. Kumar, G. Panda, M.I. Siddiqi, J. Mol. Model. 13 (2007) 99–109.
[15] A. Kumar, M.I. Siddiqi, J. Mol. Model. 14 (2008) 923–935.
[16] R.D. Cramer III, D.E. Patterson, J.D. Bunce, J. Am. Chem. Soc. 110 (1988) 5959–5967.
[17] G. Klebe, U. Abraham, T. Mietzner, J. Med. Chem. 37 (1994) 4130–4146.
[18] P. Gedeck, B. Rohde, C. Bartels, J. Chem. Inf. Model. 46 (2006) 1924–1936.
[19] M.A. Johnson, G.M. Maggiora, Concepts and Applications of Molecular Similarity, John Wiley & Sons, New York, 1990.
[20] A. Bender, J.L. Jenkins, J. Scheiber, S.C. Sukuru, M. Glick, J.W. Davies, J. Chem. Inf. Model. 49 (2009) 108–119.
[21] R.P. Sheridan, S.K. Kearsley, Drug Discov. Today 7 (2002) 903–911.
[22] MACCS Structural Keys, Symyx Software, San Ramon, CA, 2005.
[23] R. Suzuki, H. Shimodaira, Bioinformatics 22 (2006) 1540–1542.
[24] V. Kashyap, S. Sharma, V. Singh, S. Sharma, M. Saquib, R. Srivastava, A.K. Shaw, Antimicrob. Agents Chemother. 58 (2014) 3530–3532.
[25] C.A. Rivera-Marrero, J.D. Ritzenthaler, J. Roman, K.W. Moremen, Microb. Pathog. 30 (2001) 9–18.
[26] M. Clark, R.D. Cramer III, N.V. Opdenbosch, J. Comput. Chem. 10 (1989) 982–1012.
[27] SYBYL Molecular Modeling System Version 7.1, Tripos Inc., St. Louis, MO, 2005.
[28] R. Guha, J. Stat. Softw. 18 (2007) 1–16.
[29] J.H. Ward Jr., J. Am. Stat. Assoc. 58 (1963) 236–244.
[30] R Development Core Team, R: A language and environment for statistical computing. R Foundation for Statistical Computing, Vienna, Austria. ISBN 3-900051-07-0, <http://www.R-project.org/>.
[31] R.D. Cramer III, D.E. Patterson, J.D. Bunce, Prog. Clin. Biol. Res. 291 (1989) 161–165.
[32] V.N. Viswanadhan, A.K. Ghose, G.R. Revankar, R.K. Robins, J. Chem. Inf. Comput. Sci. 29 (1989) 163–172.
[33] J. Söding, A. Biegert, A.N. Lupas, Nucleic Acids Res. 33 (2005) W244–W248 (Web Server issue).
[34] A. Šali, T.L. Blundell, J. Mol. Biol. 234 (1993) 779–815.
[35] T. Darden, D. York, L. Pedersen, J. Chem. Phys. 98 (1993) 10089–10092.
[36] B. Efron, Ann. Statist. 7 (1979) 1–6.
[37] J. Felsenstein, Evolution 39 (1985) 783–791.
[38] H. Shimodaira, Syst. Biol. 51 (2002) 492–508.
[39] H. Shimodaira, Ann. Statist. 32 (2004) 2616–2641.
[40] H. Shimodaira, M. Hasegawa, Bioinformatics 17 (2001) 1246–1247.